Taylor & Francis
Taylor & Francis Group

ORIGINAL RESEARCH

OPEN ACCESS | Check for updates

scRNA-seq reveals ATPIF1 activity in control of T cell antitumor activity

Genshen Zhong[a,b#], Qi Wang[a,b#], Ying Wang[a], Ying Guo[a], Meiqi Xu[a], Yaya Guan[c], Xiaoying Zhang[d], Minna Wu[e], Zhishan Xu[e], Weidong Zhao[a], Hongkai Lian[d], Hui Wang[a], and Jianping Ye[d,f]

[a]Henan Key Laboratory of Immunology and Targeted Therapy, Henan Collaborative Innovation Center of Molecular Diagnosis and Laboratory Medicine, School of Laboratory Medicine, Xinxiang Medical University, Xinxiang, Henan, China; [b]Xinxiang Key Laboratory of Tumor Microenvironment and Immunotherapy, School of Laboratory Medicine, Xinxiang Medical University, Xinxiang, Henan, China; [c]Department of Clinical Laboratory, Xinxiang Medical University Affiliated Third Hospital, Xinxiang, Henan, China; [d]Metabolic Disease Research Center, Zhengzhou University Affiliated Zhengzhou Central Hospital, Zhengzhou, Henan, China; [e]School of Basic Medical Sciences, Xinxiang Medical University, Xinxiang, Henan, China; [f]Center for Advanced Medicine, College of Medicine, Zhengzhou University, Zhengzhou, Henan, China

ABSTRACT

ATP synthase inhibitory factor 1 (ATPIF1) is a mitochondrial protein with an activity in inhibition of F_1F_o-ATP synthase. ATPIF1 activity remains unknown in the control of immune activity of T cells. In this study, we identified ATPIF1 activity in the induction of CD8^{+} T cell function in tumor models through genetic approaches. ATPIF1 gene inactivation impaired the immune activities of CD8^{+} T cells leading to quick tumor growth (B16 melanoma and Lewis lung cancer) in ATPIF1-KO mice. The KO T cells exhibited a reduced activity in proliferation and IFN-γ secretion with metabolic reprogramming of increased glycolysis and decreased oxidative phosphorylation (OXPHOS) after activation. T cell exhaustion was increased in the tumor infiltrating leukocytes (TILs) of KO mice as revealed by the single-cell RNA sequencing (scRNA-seq) and confirmed by flow cytometry. In contrast, ATPIF1 overexpression in T cells increased expression of IFN-γ and Granzyme B, subset of central memory T cells in CAR-T cells, and survival rate of NALM-6 tumor-bearing mice. These data demonstrate that ATPIF1 deficiency led to tumor immune deficiency through induction of T cell exhaustion. ATPIF1 overexpression enhanced the T cell tumor immunity. Therefore, ATPIF1 is a potential molecular target in the modulation of antitumor immunity of CD8^{+} T cells in cancer immunotherapy. Induction of ATPIF1 activity may promote CAR-T activity in cancer therapy.

Introduction

Metabolic reprogramming through PD-1/PD-L1 antibodies is an effective strategy in cancer therapy for advanced or drug-resistant cancers. The metabolic reprogramming induces immune activities of T cells in durability, longevity, and functionality.[1,2] Energy supply is a primary factor in the control of the T cell activities, especially in the glucose-limiting tumor microenvironment, in which T cells suffer energy deficiency from low supplies of glucose and other nutrients.[3] Glucose provides energy (ATP) and building materials to support T cell survival and function.[4] The energy shortage is intensified by the exhaustion proteins (PD-L1) released from tumors.[2] Metabolic reprogramming is a potential strategy to overcome the energy shortage for energy homeostasis in T cells.[5] The metabolic remodeling is critical for the effector functions, epigenetic changes, and cell differentiation of T cells.[6,7] However, the strategy is limited by a lack of molecular targets in the metabolic reprogramming.[4,8]

ATPIF1 (IF1) is an inhibitory protein of F_1Fo-ATP synthase (ATP synthase, Complex V) that catalyzes ATP production by phosphorylation of ADP at the expense of mitochondrial potential in the energy-enriched environment.[9] The ATP synthase hydrolyzes ATP in the energy-deficient conditions to protect cells from apoptosis, in which the energy is used to maintain the mitochondrial potential. Both activities of the ATP synthase are regulated by ATPIF1 through a physical interaction.[9–11] Additionally, ATPIF1 is vital in the maintenance of mitochondrial structure.[12] It was reported that global ATPIF1 deficiency did not impact the mouse growth and breeding.[13] However, ATPIF1 inactivation protected mice from hyperglycemia in diet-induced obese mice and attenuated colitis in the mouse model.[14,15] ATPIF1 activity has been investigated in the regulation of metabolism in the neuronal cells,[16] red blood cells,[17] epithelial cells,[18] hepatocytes,[19] and tumor cells.[20] However, its role remains unclear in lymphocytes.

In this study, we analyzed Atpif1 expression in tumor infiltrating leukocytes (TILs) based on the results of single-cell sequencing (scRNA-seq) and tested ATPIF1 activity in T cells in the ATPIF1-KO mice. The results suggest that Atpif1 inactivation impaired the CD8^{+} T cell activities in proliferation, IFN-γ secretion, and resistance to exhaustion. The impact was a consequence of metabolic reprogramming in CD8^{+} T cells following the Atpif1 gene inactivation. In contrast, Atpif1

#Genshen Zhong and Qi Wang contributed equally to this work.
🅑 Supplemental data for this article can be accessed online at https://doi.org/10.1080/2162402X.2022.2114740

overexpression enhanced the antitumor efficacy of CD19-targeted chimeric antigen receptor (CAR) T cells. These results suggest that APTIF1 is a potential molecular target in the metabolic reprogramming of T-cells for cancer immunotherapy.

Materials and Methods

Cell lines

Human acute lymphoblastic leukemia CD19$^+$ NALM-6 (CRL-3273, ATCC), mouse B16-F0 melanoma (CRL-6322™, ATCC), Lewis lung cancer (CRL-1642™, ATCC) were cultured in RPMI 1640 medium (Invitrogen, USA) supplemented with 10% FBS (Gibco, USA) and 1% (v/v) P/S (Sigma-Aldrich, USA) at 37°C, 5% CO_2. CD19$^+$ NALM-6 cell line expressing Luciferase (CD19$^+$ NALM-6-luc) was generated by stably transducing fire-fly luciferase in wild-type CD19$^+$ NALM-6 cells.

ATPIF1$^{-/-}$ mice

The ATPIF1 knockout mouse was generated and identified as described in our previous studies.[12,13] The ATPIF1$^{-/-}$ mice were maintained in the pathogen-free animal facility with free access to food and water, temperature of 20 ± 2°C, humidity of 60 ± 5%, 12 h light/dark cycle/day at the Xinxiang Medical University. All the animal procedures were approved by the Institutional Animal Care and Use Committee (IACUC) of the Xinxiang Medical University. Male and female ATPIF1$^{-/-}$ mice at ages of 6–12 weeks were used in this study with the wild type (WT) littermates in the control.

CD3$^+$ T cells were isolated from the human umbilical cord blood in preparation of the CAR-T cells. The experiment design was approved by the Medical Ethics Committee in Xinxiang Medical University, and the informed consent forms were signed by the patients who gave cesarean birth before the blood collection.

Tumor growth and tumor-infiltrating T cells

Mice were implanted subcutaneously with 1×10^6/mouse of B16-F0 melanoma, Lewis lung cancer or B16-OVA melanoma cells (day 0) in the right axilla to establish the tumor-bearing mouse model. Tumor growth was monitored twice/week, and the tumor size was determined by tissue weight after collection from each mouse at about 2 weeks (B16 cancer) or 4 weeks (Lewis lung cancer), when the tumor dimension reached about 20 mm in any direction. The tumor-infiltrating lymphocytes were investigated in the excised melanoma tumors (2 mm^3 tissue) following digestion with the type II gelatinases (0.5%) for 30–40 minutes at 37°C on a shaker. The cell suspension of tumor tissues was filtered with a 70 μm filter obtain the single-cell solution, were washed twice with PBS containing 2% FBS and blocked with CD16/32 Fc block (Cat. 553142, BD Bioscience) before the analysis. The cell populations were examined with different antibodies using flow cytometry.

For adoptive T cell transfer experiment, 1×10^6 B16-OVA melanoma cells were inoculated into the right flank of Rag1$^{-/-}$ mice (n = 5, purchased from the GemPharmatech Co., Ltd. in China), and 3 days after tumor inoculation, 2×10^6 CD8$^+$ OT-I T cells or CD8$^+$ ATPIF1$^{-/-}$ OT-I T cells were injected in 150 μl of saline via the tail vein, respectively. Tumors were measured with a precision caliper every 3 days, and the tumor size was calculated.

Mitochondrial function and glycolysis

CD8$^+$ T cells were isolated from the mouse spleen and activated with CD3/CD28 antibody stimulation in the culture medium. The cells (or the CAR-T cells) were loaded at 1×10^6/well into XF24 plate, which was coated with Cell-Tak (company name, 22.4 μg/mL, in sterile water) for 20 minutes to increase the adhesion of T cells. The plate was centrifuged at $200 \times g$ (zero braking) for 1 minute to let the T cells to adhere to the culture surface. After incubation for 30 minutes at 37°C without CO_2 supplementation, Oxygen Consumption Rate (OCR) and Extracellular Acidification Rate (ECAR) were determined with the Seahorse XF Cell Mito Stress Test Kit and Seahorse XF Glycolysis Stress Test kit with the Agilent Technologies equipment. The final concentrations of inhibitors were 1 μM oligomycin, 2 μM FCCP, 0.5 μM rotenone, and antimycin A. In the ECAR assay, the final concentrations of compounds were 10 mM glucose, 1 μM oligomycin, and 50 mM 2-Deoxy-D-glucose. The readings were taken after each sequential injection of corresponding chemicals.

Targeted metabolomics

The CD8$^+$ T cells were isolated from the spleen of tumor-bearing mice, which were inoculated with B16-OVA tumor for 2 weeks (n = 6), and frozen immediately with dry ice. The energy metabolites were quantified using the LC-MS method. The analysis included 32 major metabolites of the tricarboxylic acid cycle (TCA), glycolytic pathway, pentose phosphate pathway, and oxidative phosphorylation pathway. The hierarchical clustering and quantity of the metabolites are presented to show the change in lymphocytes.

MitoTracker and ROS assay

T cells were cultured in the high glucose (HG, 4.5 g/L) medium. The mediums were prepared in glucose-free RPMI 1640 medium supplemented with glucose, 10% FBS, 1% Penicillin-Streptomycin solution. After culture for 24 h in the presence of stimulation of CD3/CD28 dynabeads (Cat. 11452D, ThermoFisher), the mitochondrial mass was examined using Mito-Tracker Red CMXRos (Beyotime, China, Cat#C1049B-250 μg), and the ROS level was determined with the DCFH-DA probe (Beyotime, China, Cat#S0033M) with flow cytometry (Beckman, CytoFLEX™).

Mitochondrial membrane potential (Δψm)

The T cells were cultured under high glucose (HG, 4.5 g/L glucose) in the RPMI-1640 medium with the addition of JC-1 in the mitochondrial membrane potential assay kit (Beyotime Biotechnology Limited Company. Shanghai, China), and incubated in the normal (O_2 concentration about 20%) condition.

After 24 h cultures with or without CD3/CD28 dynabeads (Cat. 11452D, ThermoFisher) stimulation, the T cells were collected and stained with CD3-APC/CD8-PerCP antibodies and analyzed with flow cytometry (BD, FACSCalibur). The ratio of JC-1 Red/JC-1 Green was used to indicate the Δψm of cells.

T cell proliferation

CD3$^+$ T cells were isolated from the spleen of unmanipulated WT or KO C57BL/6 mice using a negative selection T cell separation kit (Cat. 8802-6840-74, ThermoFisher). CD3$^+$ T cells were labeled with the CellTrace carboxyfluorescein diacetate succinimide ester (CFSE, Cat. C34554, ThermoFisher), and then cultured with 30 U/mL rIL-2 (Cat. 34-8021-85, eBioscience) and activated with the mouse T-activator CD3/CD28 Dynabeads (Cat. 11452D, ThermoFisher) for 96 hours under the HG conditions. The T cells were collected and stained with CD3-PE, CD8-PerCP and then analyzed with the BD FACSCalibur for evaluation of cell proliferation.

Cytokine assay

In CD8$^+$ T cells, the flow cytometry was used to detect INF-γ in the CD3$^+$ T cells after activation with the eBioscience™ Cell Stimulation Cocktail plus protein transport inhibitors (Cat. 00-4975-93, 500X). The cells were stained with CD3-PE and CD8-FITC antibody, then fixed with the eBioscience™ Fixation/ Permeabilization Diluent agents (Cat. 00-5223-56) for 1 h. After washing, the cells were stained with IFN-γ-APC antibody and then analyzed with the FACS station.

ATP test

The CD3$^+$ T cells were isolated from the spleen of WT and KO mice, cultured in a 24 well plate (2 × 10^7 cells per well), stimulated with CD3/CD28 Dynabeads. Four hours later, the cells were collected after washing in PBS. The cells were lysed, and the protein content was determined with the BCA assay (Cat. 23225, Pierce). The ATP concentration was determined using an ATP determination kits (Cat. A22066, Invitrogen) according to the protocol. The final ATP content was calculated after normalization of the ATP concentration with protein concentration.

RNA-seq of CD8$^+$ T cells

The CD8$^+$ T cells were isolated from the spleen of WT and ATPIF1$^{-/-}$ mice and then stimulated with CD3/CD28 antibody for 24 hours. After that, the cell pellets were collected and stored at TRIzol solution (Takara, Japan) and then sent to BGI (BGI, China) for RNA-seq. The data were analyzed at Dr.com platform which established by BGI. The RNA-seq data were uploaded to the NCBI with the accession number of PRJNA796630 (https://www.ncbi.nlm.nih.gov/sra/PRJNA796630).

scRNA-seq of TILs

B16-F0 melanoma cells were implanted in the right flank of male mice (n = 12). On the day 12, the tumors were dissected from the surrounding fascia, mechanically minced to approximately 1 mm^3 pieces, then the tumor tissue suspension from six mice was mixed together in each group (WT and KO). The mixed cell suspension was stored in a solution provided by the Beijing Analytical Biosciences Technology Co., Ltd., a company. The samples were sent to the company for isolation of tumor infiltrating leukocytes (CD45$^+$ cells) immediately and scRNA-seq analysis. The preparation of TILs, reverse transcription, DNA library construction, DNA sequencing, sample quality control, scRNA-seq data processing and cluster analysis were all performed by the Beijing Analytical Biosciences Technology Co., Ltd. The 10X scRNA-seq protocol was described in detail in two studies.[21,22] The raw data of scRNA-seq and TCR sequencing were uploaded to the GEO with the accession number of GSE158278. (https://www.ncbi.nlm.nih.gov/geo/query/acc.cgi?acc=GSE158278)

Construction of CD19 CAR-T and CD19-IF1 chimeric antigen receptor (CAR)

DNA fragments for scFv anti-CD19 chimeric receptors CD19-CAR or CD19-IF1 CAR were synthesized by Genescript (Nanjing, China) and cloned into a lentiviral vector (plenti-EF1A-CD19-CART-copGFP, CD19 CAR) to obtain the IF1 overexpression vector (plenti-EF1A-CD19-CART-ATPIF1-copGFP, CD19-IF1 CAR). HEK293T cells (Thermo Fisher) were transfected with the control vector lenti-CD19 CAR or expression vector lenti-CD19-IF1 CAR along with packaging plasmid pMD2.G (Addgene 12259) and psPAX2 (Addgene 12260). Lentivirus was harvested from the cell culture supernatant after 48–72 hours of incubation by filtering through 0.45 μm filter followed by ultracentrifugation and stored at −80°C for further use.

Lentiviral transduction, CAR T-cell production, and proliferation

Single nucleated cells were isolated from the human umbilical cord blood (n = 3) using the Ficoll Lymphocyte Isolation Solution (TBD, Tianjin, China) by centrifugation. The cells were used in preparation of T cells through sorting with the Human CD3 Positive Selection Kit (Cat. 8802-6830-74, Invitrogen). The T cells were stimulated with HuCD3/CD28/CD2 T cell Act (Cat. 10970, Stemcell) for 24 h. The T cells were then incubated in a complete RPMI 1640 medium containing hIL-2 (200 U/mL) and 10% FBS (Gibco) for activation. On the following day, the T cells were infected with the lentivirus (CD19 CAR and CD19-IF1 CAR) containing the target gene and GFP at a ratio of MOI = 5:1 of virus vs. cells. The transfected T lymphocytes were amplified and cultured in an incubator of 37°C with 5% CO$_2$ to obtain CAR-T cells. Five days after lentivirus infection, GFP$^+$ cells were analyzed, and Goat anti-Mouse IgG (H + L) Cross-Adsorbed Secondary Antibody (Alexa Fluor 647, Cat#A-21235, Invitrogen) was used to detect

the positive ratio of CAR-T cells by flow cytometry. After 2 weeks cultivation, the expanded CAR-T cells were used in the follow-up experiments.

CAR-T cells analysis

In order to analyze CAR-T cell function, several groups of coculture experiments were carried out. Before the experiment, the CAR-T cells were set down overnight, and 2×10^5 CD19-CAR-T cells or CD19-IF1-CAR-T cells were cultured with 2×10^5 CD19$^+$ Nalm6-luc cells in a 24 well plate in 2 ml/well RPMI 1640 complete medium for 24 h. Expression of PD-1, TIM-3, LAG-3, Granzyme-B, and the T subset population (T_{Naive}: CD45RA$^+$CD45RO$^-$, T_{CM}: CD45RA$^-$CD45RO$^+$CCR7$^+$, T_{EM}: CD45RA$^-$CD45RO$^+$CCR7$^-$, T_{SCM}: CD45RA$^+$CD45RO$^+$) were analyzed in CAR-T cells by flow cytometry. The anti-human antibodies were CD3-APC-Cy7 (Cat. 317341, Clone: OKT3, Biolegend), CD4-APC (Cat. 357407, Clone: A161A1, Biolegend), CD8-PB450 (Cat. 344717, Clone: SK1, Biolegend) or CD8-PE (Cat. 344705, Clone: SK1, Biolegend), PD-1-APC (Cat. 367405, Clone: NAT105, Biolegend), LAG-3-PE (Cat. 369305, Clone: 11C3C65, Biolegend), TIM-3-Percp-Cy5.5 (Cat. 345015, Clone: F38-2E2, Biolegend), CD45RA-PB450 (Cat. 304117, Clone: HI100, Biolegend), CD45RO-PerCP (Cat. 304251, Clone: UCHL1, Biolegend), CCR7-APC-F750 (Cat. 353245, Clone: G043H7, Biolegend), Granzyme B-PE (Cat. 372207, Clone: QA16A02, Biolegend)

In the cytotoxicity test, the un-transfected T cells (UT), CD19 CART, and CD19-IF1 CAR-T were cocultured with 1×10^4 CD19$^+$ Nalm6-luc cells in a 96 well plate at different E:T ratio (5:1, 3:1, 1:1, 1:2). After 24 hours, the tumor cell lysis rate was analyzed with the firefly luciferase activity (Beyotime, one lumitm II firefly luciferase reporter gene detection kit). The cell supernatants were collected and cytokines (such as IFN-γ and IL-2) were detected with ELISA (IL2: Cat. 88-7025-22 and IFN-γ: Cat. 88-7316-22, Invitrogen). Due to the different CAR$^+$ ratio in CD19 CAR-Ts and CD19-IF1 CAR-Ts in the experiment, the input cell numbers for each experiment of CAR-Ts were normalized, and the samples were prepared with the same number of transduced CAR$^+$ cells for CD19 CAR-Ts and CD19-IF1 CAR-Ts.

In vivo experiment of CAR-T cell

Six- to eight-week-old NCG mice (NOD/ShiLtJGpt-Prkdc^{em26Cd52}Il2rg^{em26Cd22}/Gpt, Strain NO. T001475, GemPharmatech, Nanjing, China) were housed and tested under pathogen-free conditions. Eighteen NCG mice were randomly divided into three groups (n = 6), the UT group (Untransfected T group), the CD19 CAR-T group, and CD19-IF1 CAR-T group. Mice were intravenously injected with 1.2×10^6 Nalm6-luc cells via the tail vein at day 0. The mice were treated with 1.2×10^6 UT cells, CD19-CAR-T cells, or IF1-CD19-CAR-T cells at the day 6. Status of the mice was observed, and their survival period was recorded. At days 22 and 28, peripheral blood (PB) was collected from the mouse tail, and the absolute CD19$^+$ NALM-6 numbers were

determined using the flow cytometry with the 123count™ eBeads (Thermo Fisher, Cat#: 01–1234-42) as described in our previous study.[23] At day 35 after NALM-6 inoculation, the peripheral blood was collected from the mice, and the CD4$^+$ and CD8$^+$ subsets of T cells were counted with the 123count™ eBeads.

Statistical analysis

The data are presented as the mean ± SD. All of *in vitro* studies were repeated at least three times with consistent results, and the data were analyzed with an unpaired two-tailed t-test. In the *in vivo* studies, the data were analyzed with the Post Hoc tests using ANOVA of the SPSS 20.0 software package. $p < .05$ was considered statistically significant. FlowJo 10.0 was used to analyze the flow cytometry results.

Results

Antitumor efficacy of CD8$^+$ T cells is impaired in ATPIF1-KO mice

To understand ATPIF1 activity in T cells, we examined Atpif1 expression in individual T cells based on our scRNA-seq data of WT mice. The expression was detected in T cells and other cell types including B cells, macrophages, and dendritic cells (Figure 1a). The Atpif11 expression was compared with CD3e expression to understand the expression pattern in T cells (Figure 1b). The data suggest that the expression level was positively associated with CD3e in some but not all T cells, which suggests heterogenicity in T cell population. To understand the heterogenicity, the expression was examined in four T cell subsets. A difference was observed with the highest in naive T cells (T_na) followed by T proliferation cells (T_pro), T_IL17a cells (T_IL17a), and central memory T cells (T_cm) (Figure 1c). To study the impact of ATPIF1 on T cells, tumor immunity was tested in the ATPIF1-KO (ATPIF1$^{-/-}$) mice, which were made by our laboratory as described in other studies.[14,15] The KO effect was confirmed by decreased ATPIF1 protein in the spleen lymphocytes (**Fig. S1**). The knockout mice exhibited no difference from the wild type (WT) mice in growth and reproduction.[13]

The antitumor immunity was tested in the KO mice against two types of tumors, B16 melanoma, and Lewis lung cancer (LLC). The B16 tumor growth was significantly enhanced in the KO mice with a larger tumor size at 2 weeks. The tumor weight was increased in the KO mice by 2-fold on average ($p = .0079$, figure 1d). A similar increase was found in LLC tumor in the KO mice at 1.8-fold in tumor weight relatively to that of WT mice ($p = .027$, Figure 1e). To elucidate the T cell activity in the phenotype, the KO mice were bred with OT-I mice to get the ATPIF1-KO OT-I CD8$^+$ T cells. In B16-OVA cell xenografted Rag1$^{-/-}$ mice, the ATPIF1-KO group exhibited more tumor growth than the WT group ($p = .008$, Figure 1f). The corresponding tumor weight in B16, LLC, and B16-OVA xenografted experiment is summarized in Figure 1g–i. These data suggest that ATPIF1 inactivation impaired the tumor immunity in the KO mice in favor of
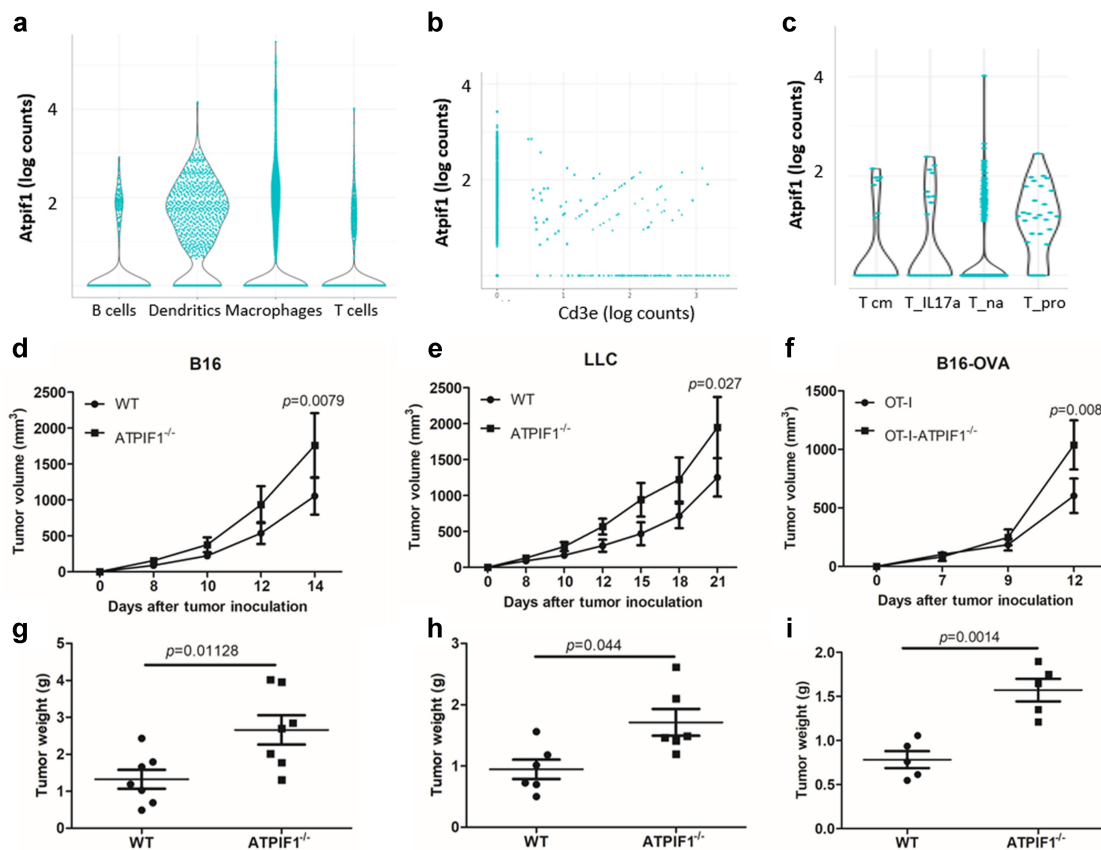
Figure 1. Antitumor activity is impaired in ATPIF1$^{-/-}$ mice. (a) Atpif1 expression in immune cells by analysis of scRNA-seq data of normal WT mice. (b) Atpif1 expression was compared with Cd3e expression for quantification of the expression in T cells by scRNA-seq data of normal mice. (c) Atpif1 expression in subsets of T cells including central memory T cells (T_cm), IL-17a expressing T cells (T_IL17a), naive T cells (T_na) and proliferative T cells (T_pro) based on the scRNA-seq data. (d and g) Increased B16 melanoma cancer growth in ATPIF1$^{-/-}$ mice (n = 7). (e and h) Increased Lewis lung cancer growth in ATPIF1$^{-/-}$ mice (n = 6). The tumors were engrafted subcutaneously and examined for tumor weight on day 14 (B16 melanoma) and 21 (Lewis lung cancer), respectively. (f and i) Dependence of tumor immunity on CD8$^+$ T cells. Rag1$^{-/-}$ mice were xenografted with B16-OVA melanoma tumor (1 × 10^6) for 3 days, then the OT-I CD8$^+$ T cells and ATPIF1$^{-/-}$ OT-I CD8$^+$ T cells (2 × 10^6) were adoptive transferred via tail vein to test the antitumor efficacy. Nine days later, the mice were sacrificed for tumor size analysis with ANOVA (n = 5). The p value as indicated, and p < .05 indicated significant difference.

tumor growth, which was related to dysfunction of CD8$^+$ T cells.

Function of CD8$^+$ T cells is retarded in KO mice

Above data demonstrated that the CD8$^+$ T cells exhibited a decreased antitumor activity in the KO mice. Mitochondrial activities were examined in the cells to understand mechanism of the decrease. F_1F_o-ATP synthase makes as well as hydrolyzes ATP, and both activities rise in the absence of ATPIF1.[24] Such alterations were not verified in T cells before this study. Mitochondrial potential ($\Delta\psi m$) and intracellular ATP content were examined to address the issue. CD8$^+$ T cells were isolated from the spleen and used in the following experiments. $\Delta\psi m$ was determined in the intact cells using JC-1, a lipophilic and cationic dye for detection of mitochondria membrane potential.[25] The KO cells exhibited normal $\Delta\psi m$ in the resting condition as shown by the JC-1 red/green ratio (Figure 2a). In the activation condition, the KO cells had a higher $\Delta\psi m$ following a sharp $\Delta\psi m$ reduction in the WT cells. The KO cell had more intracellular ATP content in the resting and

activated conditions (Figure 2b), supporting an increase in ATP synthesis. Additionally, IF1 plays a role in the modulation of mitochondrial cristae.[12,26] Mitochondrial mass was determined using MitoTracker staining. The KO cells had a lower mitochondrial mass in the resting condition as indicated by MFI (Figure 2c). However, the difference disappeared after cell activation as the WT cells displayed a remarkable mass reduction in response to the activation (Figure 2c). ROS, determined with the fluorescent probe DCFH-DA, revealed that the KO cells had a normal ROS level in the resting condition, but less ROS in the activated status (Figure 2d). Manipulation of ROS with N acetylcysteine (NAC) *in vivo* could not remove the difference in tumor growth between the KO and WT mice (**Fig. S2**), suggesting that ROS may not be responsible for the difference in tumor immunity. IFN-γ secretion and cell proliferation were examined to understand the impact of mitochondrial alteration. Following activation, the KO cells produced less IFN-γ as determined by the flow cytometry (Figure 2e, p < .0001). The proliferation activity was decreased as well in the CFSE-labeled experiment (Figure 2f). These data demonstrate that ATPIF1 deficiency
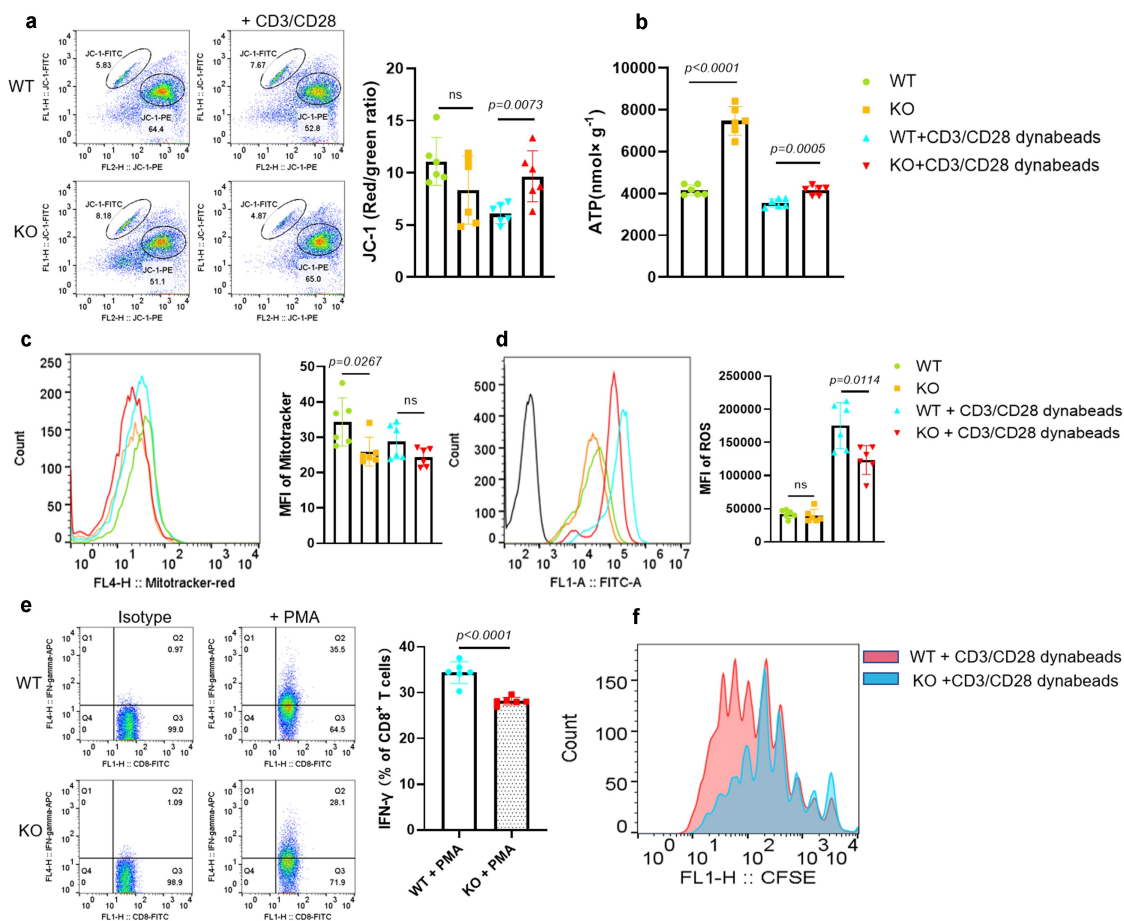
Figure 2. Changed characteristic of CD8+ T cells in ATPIF1-KO mice. (a) Increased mitochondrial membrane potential in KO cells after CD3/CD28 Dynabeads stimulation. The ratio of red and green signals of JC-1 was calculated to determine the mitochondrial potential and a comparison was made between the KO and WT cells for the change. (b) Increased ATP content in KO CD8+ T cells. The CD8+ T cells were lysed and the intracellular ATP was determined using the assay kit according to the protocol. (c) Decreased mitochondrial mass. The signals were quantified with flow cytometer and the mean fluorescence intensity (MFI) of Mitotracker was calculated and plotted in the bar figures. (d) Decreased ROS in KO CD8+ T cells after CD3/CD28 Dynabeads stimulation. The signals were quantified with flow cytometer and the mean fluorescence intensity (MFI) of DCFH-DA was calculated and plotted in the bar figures. The black-line peak in graph D was the negative control without the staining of DCFH-DA. (e) IFN-γ content was decreased in KO CD8+ T cells. CD3+ T cells were stimulated with 1× Cell stimulation cocktail (plus protein transport inhibitors) for 24 hours. Cultures were then harvested and stained with CD3 and CD8 antibody, then fixed and permeabilized with fixation buffer and permeabilization buffer. Cells were further stained with anti-mouse IFN-γ antibody. Cells in the CD3 + T cells gate were used in the analysis. (f) Delayed proliferation of CD8+ T cells after IF1 deficiency. CD3+ T-cells were isolated from the spleen and labeled with CFSE. The cells were stimulated with CD3/CD28 Dynabeads in the culture medium, and the CD8+ T cells were gated for the CFSE.

reprogrammed the energy metabolism in CD8+ T cells for a reduced antitumor efficacy.

Reprogrammed glycolysis and OXPHOS in KO cells

Glucose is the major fuel in T cells for ATP production in the glycolysis and OXPHOS pathways. The two pathways were examined in CD8+ T cells by measuring the oxygen consumption rate (OCR for OXPHOS) and the extracellular acidification rate (ECAR for aerobic glycolysis) using the Seahorse equipment. The KO cells presented a low activity in OXPHOS in both the resting and activated states (Figure 3, a and b. $p < .05$). The reduction led to a decrease in the spare respiratory capacity (SRC) in the KO cells (Figure 3, a and b). The KO cells had a low activity in glycolysis at the resting state (Figure 3c. $p < .05$) but exhibited much more activity in the activated state for a huge rise in ECAR (Figure 3d). The glycolytic reserve (GR) was significantly higher in the KO cells in the activated state (Figure 3, c and d. $p < .01$). An

increase in SRC is a character of energy metabolism in the memory T cells and in GR is a feature of the effector T cells.[27,28] The data suggest that glucose metabolism is reprogrammed in the KO cells for enhanced glycolysis and decreased OXPHOS.

Targeted metabolomics was used to investigate the metabolic reprogramming in the KO cells. CD8+ T cells (1×10^7) were purified from the spleen of tumor-bearing (B16-OVA) mice through FACS-based sorting. Metabolites were targeted in the energy metabolism pathways using the liquid chromatography-mass spectroscopy (LC-MS). Metabolites include those in the tricarboxylic acid cycle (TCA), glycolytic pathway, OXPHOS, and pentose phosphate pathway. The metabolite profile revealed that the KO cells had a higher activity in glycolysis and the pentose phosphate pathways for an increase in D-Glucose 1-phosphate, D-Glucose 6-phosphate, α-D-Ribose 5-phosphate, and coenzyme A (Figure 3, e and f, raw data are summarized in **Table S1**). The TCA cycle activity was decreased in the KO cells for a reduction in acetoacetyl-CoA and acetyl-CoA. The
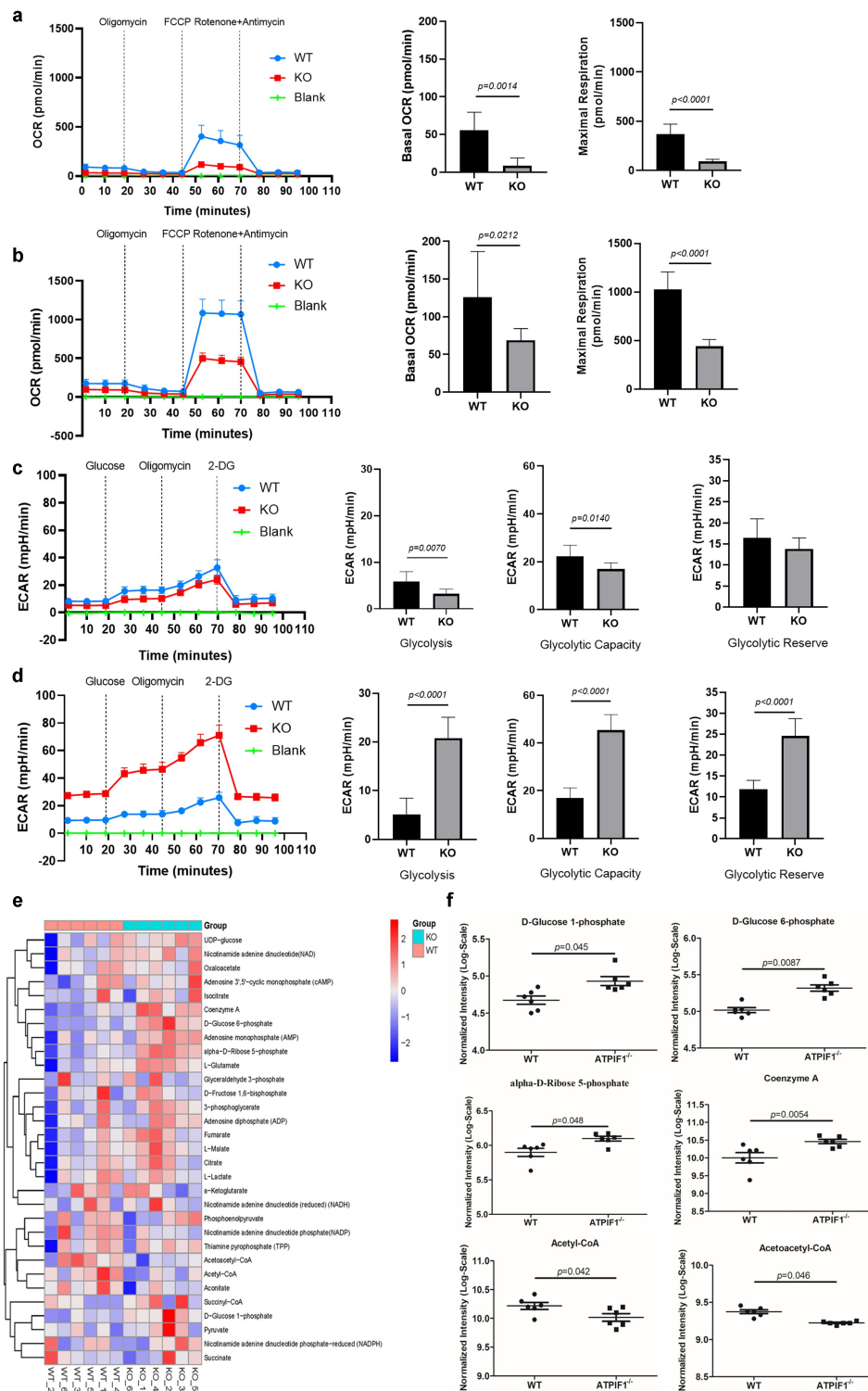
Figure 3. KO cells are reprogrammed for active glycolysis and decreased OXPHOS. (a) Oxygen consumption rate (OCR) in the resting CD8$^+$ T-cells. Basal and maximal OCR was determined in the resting cells (without CD3/CD28 antibody stimulation). (b) OCR in the activated cells. The CD8$^+$ T-cells were stimulated with CD3/CD28 for 24 h in the culture and then examined for the basal and maximal OCR. (c) Extracellular acidification rate (ECAR) in the resting T-cells. (d) ECAR in the activated T-cells. The glycolysis, glycolytic capacity and glycolytic reserve were calculated in cells at the basal or activated states. (e) Heatmap of targeted metabolomics focus on the 31 intermediate products of glucose in the tricarboxylic acid cycle (TCA), glycolytic pathway, OXPHOS and pentose phosphate pathway in CD8$^+$ T cells of KO and WT mice. The CD8$^+$ T cells were isolated from the spleen of B16-OVA tumor-bearing mice and analyzed as described in the Methods section (n = 6). (f) Quantification of 6 intermediate products in the targeted metabolomics. The data represents mean ± SD (n = 6) with p value < .05.

data provide an extra support that the KO cells were reprogrammed for active aerobic glycolysis and inactive OXPHOS, which may account for the ATP elevation in KO cells.

RNA-seq analysis of CD8+ T cells reveals the decreased cytokine production

To explore the molecular mechanisms of the impaired T cell functions, RNA-sequencing (RNA-seq) was conducted in CD8+ T cells, which were isolated from the B16 tumor-bearing mice. The principal component analysis (PCA) showed that KO cells displayed a significant difference in gene expression profile (Figure 4a), with 514 genes up-regulated and 855 genes down-regulated in reference to the WT cells. The differentially expressed genes (DEGs) suggested that the immune system, signal transduction, and transport and catabolism were significantly changed in the KO cells according to the Kyoto Encyclopedia of Genes and Genomes (KEGG) (Figure 4b). The KO cells exhibited an alteration in the cytokine–receptor interaction and cell differentiation (Figure 4c). The heatmap of selected DEGs (all p-value < 0.001 as compared) indicated a reduction in the expression of IFN-γ, Gzma, Il2ra, and Id2 in the KO cells (Figure 4d). A gene set enrichment analysis (GSEA) was performed on all genes to complement the inherent limitations of DEGs analysis. The results demonstrated that the ribosome (FDR = 0.027, FDR = false discovery rate) and ribosome biogenesis (FDR = 0.026) were changed significantly in the KO cells, and OXPHOS were also changed in KO cells (Figure 4e). Overall, the RNA-seq data provide a support in gene expression for ATPIF1 modulation of T cell activities in multiple aspects, including cytokine production, metabolism, ribosome biogenesis, and cell differentiation.

scRNA-seq ATPIF1 inactivation promotes CD8+ T cell exhaustion in TILs

Above data consistently suggest that the ATPIF1 inactivation may generate an impact in CD8+ T cells to decrease the tumor immunity. To investigate the impact on subsets of CD8+ T cells, tumor infiltering leukocytes (TILs) were isolated from the melanoma using a CD45 antibody and analyzed by 10X Genomics scRNA-seq technology according to the studies of liver cancer[21] and breast cancer.[29] In the experiment, TILs were prepared from the pooled samples of six mice in each group and 18467 cells (8408 in KO and 10059 in WT cells) were analyzed (**Fig. S3**). The qualified data were obtained from 6007 cells in KO and 8010 cells in the WT group (**Table S2**). The violin chart and the principal component analysis (PCA) suggest an excellent quality control in the scRNA-seq assay (**Fig. S4, A and B**). The T-distributed random neighborhood embedding (tSNE) and the uniform manifold approximation and projection (UMAP) graph revealed similar cluster landscapes in the KO and WT mice (**Fig. S4, C and D**).

ATPIF1 inactivation promoted exhaustion in the proliferation (CD8T_Proliferation_KO) and effector memory (CD8T_EffectorMemory_KO) subsets of CD8+ T cells. T cells were divided into eight subclusters in TILs according to the scRNA-seq data (Figure 5a). The marker genes for each cluster are listed in the supplementary file (**Fig. S5**). The KO cells exhibited a higher expression of the exhaustion markers including PD-1, LAG-3, and TIGIT in the subsets of proliferative and effect memory CD8+ T cells (Figure 5b). To verify the results, their protein levels were examined in CD8+ T cells of the spleen, lymph node (LN), and TILs using flow cytometry. Up-regulation of exhaustion markers (PD-1 or LAG-3) was confirmed in the KO T cells, and a difference was observed among the three tissues (Figure 5, c, d and e). PD-1 but not LAG-3 was upregulated in the spleen and tumor, LAG-3 (not PD-1) was upregulated in the lymph node. Tim-3 upregulation was not observed in T cells. Subsets of T cells were examined using flow cytometry. The percentage of T_{CM} (CD44+ CD62L+ CD8+) was decreased in the TIL of KO mice (p = .0264, compared to that of WT, figure 5f). These data consistently support that the functions of CD8+ T cells were impaired in TILs of ATPIF1-KO mice.

Overexpression of ATPIF1 promotes CD19-CAR-T function

Above results demonstrated that ATPIF1 may promote the antitumor activity of CD8+ T cells. To test the possibility, ATPIF1 overexpression was tested in T cells for antitumor efficacy. Chimeric Antigen Receptor (CAR)-T cells are effective in inhibition of CD19+ B cell malignancy.[30] The human T cells were infected by an IF1 overexpression lentivirus, which was generated with the CD19-BBζ lentiviral vector for expression of recombinant IF1 (Figure 6a). The IF1 overexpression CAR-T (CD19-IF1 CAR-T) was produced and tested for tumor killing activity (**Fig. S6**). As shown in Figure 6b, the over expression CAR-T showed similar expansion curve as compared to that of control CAR-T (CD19 CAR-T). In the coculture system, the overexpression CAR-T did not exhibit a significant difference in the killing efficacy of NALM-6^{Luc+} tumor cells (Figure 6c). However, their activity in expression of IFN-γ and IL2 was altered. The IFN-γ content in the supernatant of overexpression CAR T was significantly higher than that of the control group (Figure 6d), whereas the IL-2 level was significantly lower than that of the control CAR T (Figure 6e). Granzyme B expression was higher in the overexpression CAR T over the control (figure 6f). Interestingly, the percentage of CD8+ CAR-T cells were increased and the CD4+ CAR-T cells were decreased in the overexpression CAR-T cells relative to the control, suggesting that the IF1-overexpression might change differentiation of CAR-T subsets upon challenged with the NALM-6 tumor cells (Figure 6g). The exhaustion markers of PD-1, LAG-3, and TIM-3 were all decreased in the subset of CD4+ CAR-T cells. However, the expression of PD-1 and LAG-3 was increased in CD8+ CAR-T cells (Figures 6h and 6i, the gating strategy was shown in **Fig. S7**). Subpopulations of T cells were increased in T_{CM} (CD45RO+CD45RA−CCR7+) and T_{SCM} (CD45RO+CD45RA+) by the overexpression. The subpopulations of T_{Naive} (CD45RO−CD45RA+) and T_{EM} (CD45RO+CD45RA−CCR7−) were decreased by the overexpression (Figures 6j and 6k, the gating strategy was shown in **Fig. S8**). This group of data suggests that IF1 overexpression
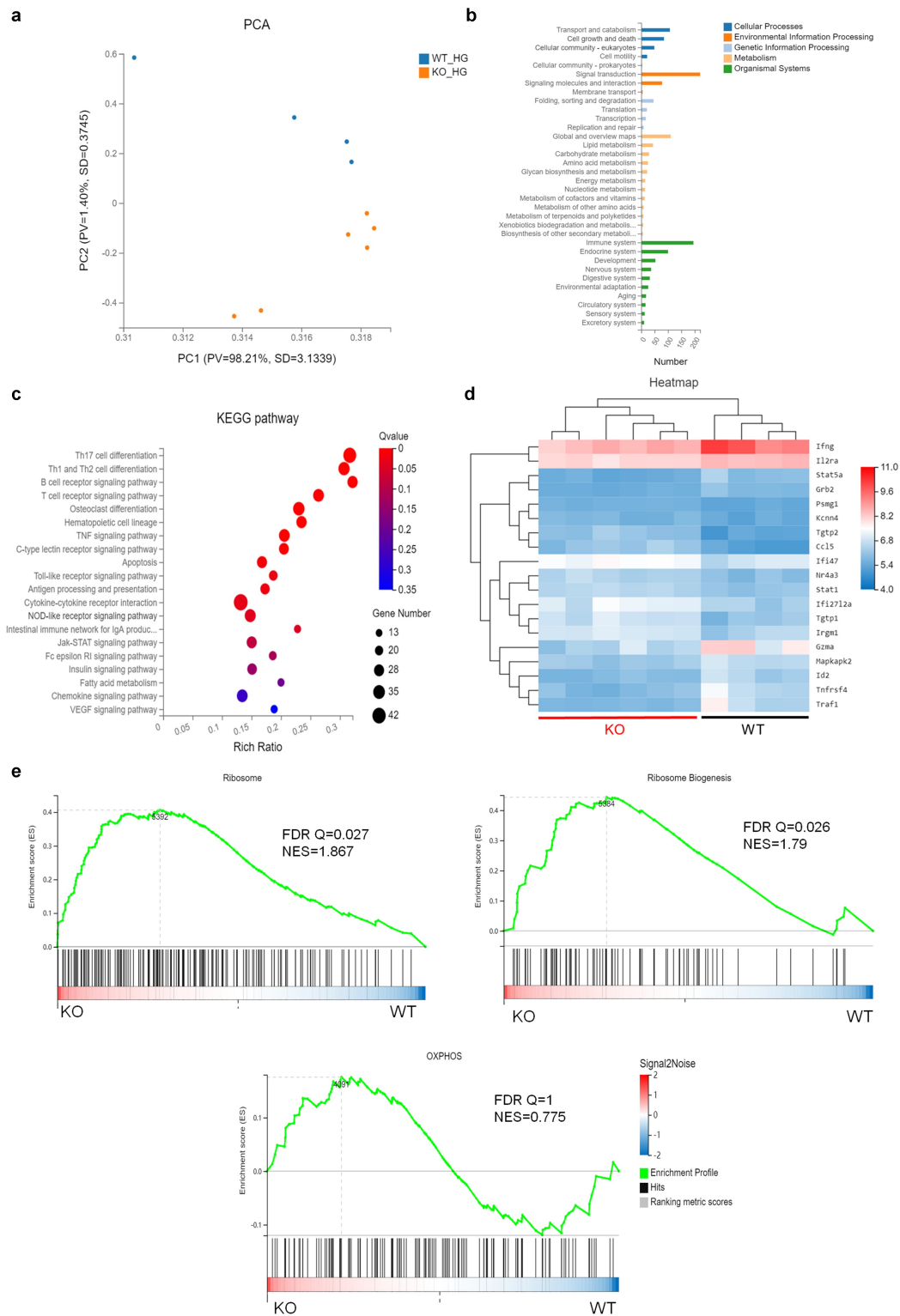
Figure 4. RNA-seq of CD8^{+} T cells in TILs. Cytokine production and immune cell differentiation were investigated in CD8^{+} T cells of TILs isolated from the B16 tumor. RNA-seq was employed to examine gene expression profile in the T cells. (a) The principal component analysis (PCA) of CD8^{+} T cells after CD3/CD28 antibody stimulation. PCA revealed that the CD8^{+} T cells of WT and KO mice formed distinct clusters. Each symbol represents a biologic sample (Blue circle, WT; Orange circle, KO). (b) KEGG pathway enrichment analysis differentially expressed genes (DEGs) in CD8^{+} T cells. (c) Bubble plot of top 30 enrichment of KEGG pathways. Advanced bubble chart shows enrichment of DEGs in signaling pathways. Y-axis represents pathway, and X-axis represents rich factor (rich factor = counts of DEG enriched in the pathway/amount of all genes in background gene set). Size and color of the bubble represent DEG counts enriched in the pathway and enrichment significance, respectively. (d) Hierarchical clustering of certain selected significantly changed DEGs between the WT and KO CD8^{+} T cells ($p < .0001$). The sample parts are listed on the primary x-axis, while DEGs are listed on the y-axis with their expression ratios (log2) expressed per the color gradient shown. (e) GSEA enrichment plots for three hallmark gene sets enriched in the CD8^{+} T cells based on the whole transcription of RNA-seq. GESA analysis of Ribosome, Ribosome biogenesis, and OXPHOS was demonstrated. NES, normalized enrichment score; FDR, false discovery rate.
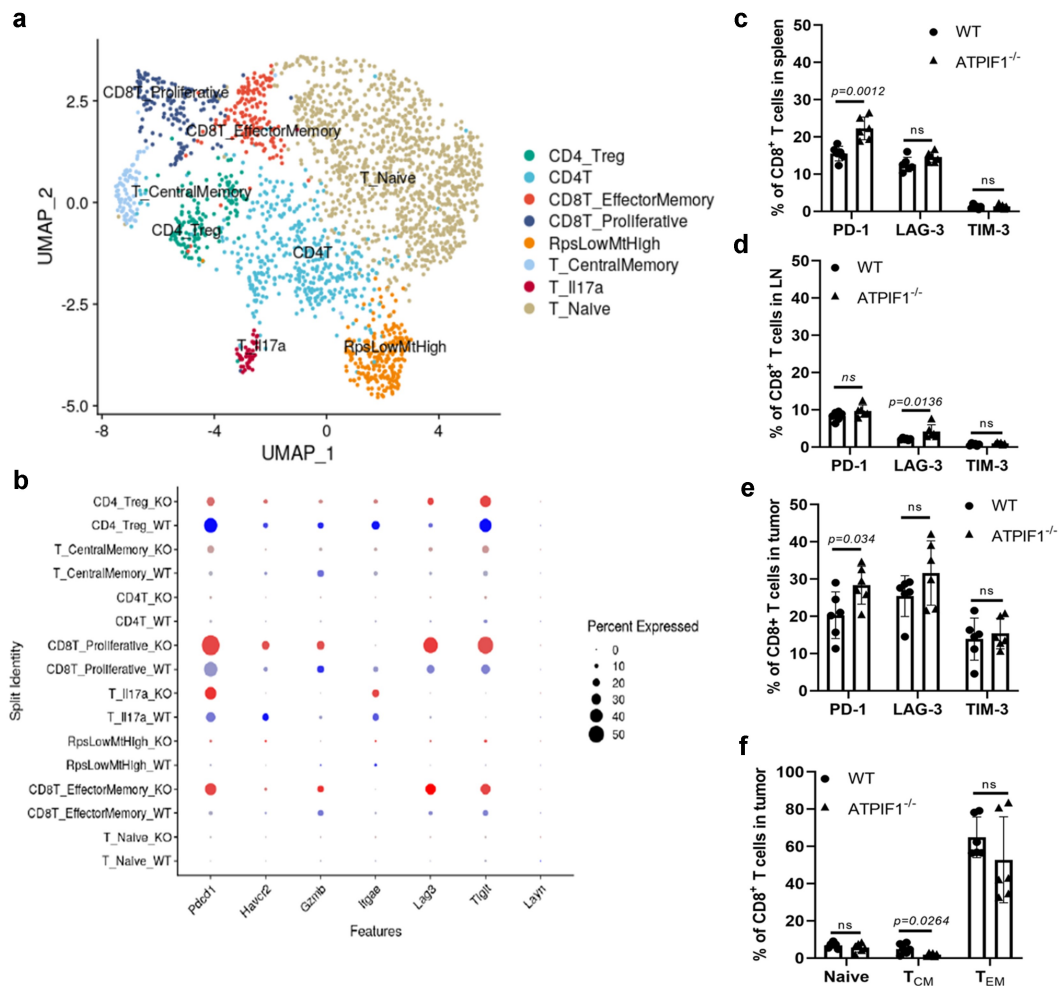
Figure 5. scRNA-seq analysis of TILs. ATPIF1-deficiency increased the exhaustion of CD8$^+$ T cell and decreased the formation of central memory CD8$^+$ T cell in B16 tumor. (a) t-SNE cluster map of T cells based on the canonical markers in scRNA-seq. Eight T cell subclusters were identified in the graph. (b) Increased percentage of exhaustion markers in the cluster of CD8$^+$ T proliferative-subcluster of KO mice in the scRNA seq analysis. (c), (d) and (e), the expression of exhaustion markers in T cells. CD8$^+$ T cells were isolated from the spleen, LN or tumor and expression of the exhaustion markers (PD-1, LAG-3 and TIM-3) were analyzed with flow cytometry. (f) Percentage of the central memory CD8$^+$ T cells was decreased in the B16 tumor of ATPIF1$^{-/-}$ mice. CD44^{lo}CD62L^{hi} CD8$^+$ T cells was defined as Naïve cell, CD44^{hi}CD62L$^-$ CD8$^+$ T cells were defined as T_{CM}, and CD44$^{+/mod}$CD62L$^-$ T cells defined as were T_{EM}.

changed cytokine production and subpopulation differentiation in CAR-T cells.

To investigate the influence of IF1 overexpression in energy metabolism of CAR-T cells, glucose metabolism in the glycolysis and oxidative phosphorylation pathways was examined using the Seahorse equipment for ECAR and OCR. As shown in Figure 7, the overexpression of CAR-T cells exhibited a decrease in glycolysis and glycolytic capacity as compared to the control (Figure 7a). However, the oxidative phosphorylation was enhanced by the overexpression as indicated by the increased OCR value (Figure 7b). The data suggest that IF1 overexpression remodeled the energy metabolism in CAR-T cells.

IF1 overexpression enhanced antitumor efficacy of CAR-T in vivo

To evaluate the impact of IF1 overexpression in CAR-T function in vivo, CAR-T was injected into tumor-bearing NCG mice via the tail veil. The tumor-bearing mice were generated by implantation of 1.2×10^6 NALM-6 leukemia cells/mice (CD19 antigen detection in NALM-6 cell was shown in Fig. S9). The CAR-T injections were made at day 6 of tumor implantation (Figure 8a). At day 22, the peripheral blood was collected and the absolute leukemia cells (CD19$^+$ NALM-6 cells) were determined using flowcytometry, and the number was significantly less in the IF1 overexpression group (Figure 8b). At day 28, the leukemia cells remained less in the overexpression group (Figure 8c), suggesting the improved antitumor efficacy of IF1 overexpression CAR-T. At day 35, the absolute count of CD4$^+$ and CD8$^+$ T cells were determined in the peripheral blood by flow cytometry. CD4$^+$ T cells were not different (Figure 8d), but CD8$^+$ T cells were higher in the overexpression group (Figure 8e), indicating that the antitumor activity of CD8$^+$ CAR-T cells was enhanced by IF1 overexpression. The mouse survival rate suggests that IF1 overexpression significantly increased the antitumor efficacy of CAR-T cells and raised the survival time of tumor-bearing
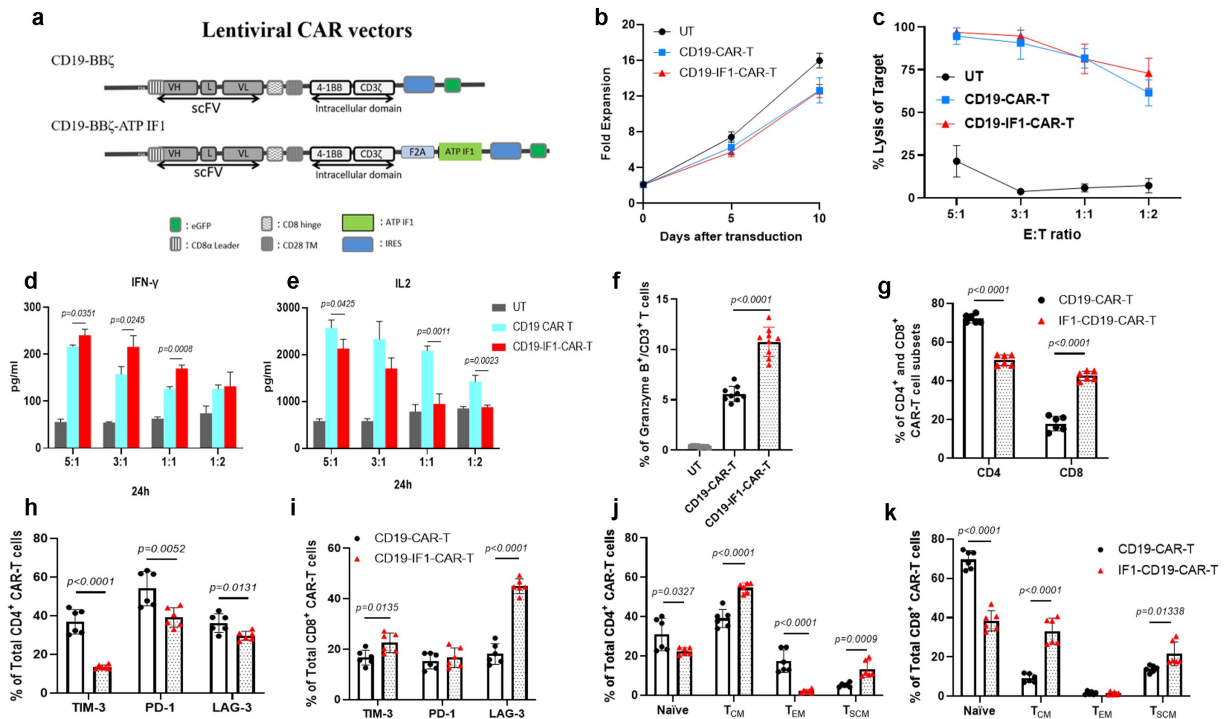
Figure 6. ATPIF1 overexpression in CD19 CAR-T cells. Cytokine expression and T cell subsets were investigated in T cells after ATPIF1 overexpression in CAR-T cells in vitro. (a) Schematic figures showing Lentiviral vector constructs of CD19 CAR-T and CD19-IF1 CAR-T. (b) Expansion of UT, CD19 CAR-T and CD19-IF1 CAR-T in the culture. (c) Lysis ratio of UT, CD19 CAR-T and CD19-IF1 CAR-T on NALM-6Luc+ in different E:T ratio after 24-hour coculture. Lytic function of CAR-T cell was tested in the bioluminescent killing assay in a 96-well microplate. Results are expressed as mean ± SD of triplicates from 3 separate experiments. (d) and (e), the IFN-γ and IL-2 content. The culture supernatant of UT, CD19 CAR-T and CD19-IF1 CAR-T with NALM-6 were collected after 24-hour coculture and the IL-2 and IFN-γ were determined using ELISA. (f) The percentage of Granzyme-B in CD3$^+$ T cells. The cells of UT, CD19 CAR-T and CD19-IF1 CAR-T were cocultured with NALM-6 for 24 hours, then the Granzyme B expression in CD3$^+$ T cells were detected using flow cytometry. (g) Percentage of CD4$^+$ and CD8$^+$ CAR-T cells after coculture with NALM-6. (h) and (i), expression of TIM-3, PD-1 and LAG-3 in CD4$^+$ or CD8$^+$ CD19 CAR-T and CD19-IF1 CAR-T cells. (j) and (k), subsets of CAR T cells after coculture with NALM-6. The percentage of different subsets in CD4$^+$ or CD8$^+$ CAR-T cells were determined using flow cytometer with the antibodies. The markers for different subsets of CAR-T cells were as following: T_{CM} (CD45RO$^+$CD45RA$^-$CCR7$^+$), T_{SCM} (CD45RO$^+$CD45RA$^+$), T_{Naive} (CD45RO$^-$CD45RA$^+$) and T_{EM} (CD45RO$^+$CD45RA$^-$CCR7$^-$).

mice (figure 8f). This group of data suggests that IF1 activation in CAR-T increased the number and antitumor activity of CD8$^+$ cell *in vivo*.

Discussion

The current study suggests that ATPIF1 is a potential candidate for molecular targets in the induction of antitumor activity of CD8$^+$ T cells. This study reports that the CD8$^+$ T cell activities were impaired in the ATPIF1-KO mice, which has not been reported yet according to a keyword search in the PubMed database. ATPIF1 inactivation in T cells led to a decrease in tumor immunity in the tumor-bearing mice. Overexpression of ATPIF1 in CAR-T cells increased the antitumor immunity in NALM-6 tumor-bearing mice. The data demonstrates a role of ATPIF1 in the regulation of T cells function.

The conclusion is supported by scRNA-seq analysis of TILs, in which the decreased T cell activities in KO mice were observed with an increased expression of exhaustion markers and decreased expression of IFN-γ. scRNA-seq was employed to determine the subpopulation of CD8$^+$ T cells in TILs, which led to the characterization of eight major subsets of T cells. In these subclusters, mRNA expression of exhaustion markers, such as PD-1, LAG-3, and TIGIT, were significantly increased in the CD8$^+$ T proliferative and effector-memory subcluster,

indicating that ATPIF1 inactivation led to the exhaustion of CD8$^+$ T cells for the decreased antitumor efficacy. The increased PD1 and LAG-3 were confirmed at the protein levels with flow cytometry in the T cells isolated from TILs, spleen, and lymph nodes. The heatmap, KEGG pathway, and GSEA analysis based on the RNA-seq data suggest that the decreased expression of cytokine genes (such as IFN-γ and Gzmb) was associated with the significant changes in ribosome or ribosome biogenesis-related genes. This indicates that ATPIF1 knockout reduced the protein synthesis, which may count for the decreased IFN-γ expression in the KO cells. *Id2* (inhibitor of differentiation-2) expression was decreased significantly in the KO cells as shown in the heatmap of RNA-seq, which may be a reason for decreased proliferation and antitumor activity of KO T cells. It was reported that *Id2* was closely related to CD8$^+$ T cell function and differentiation.[31,32]

Our data reveal that energy metabolism was reprogrammed in CD8$^+$ T cells of ATPIF1-KO mice for enhanced glycolysis in ATP production. Glycolysis was enhanced in CD8$^+$ T cells of KO mice for ATP production as indicated by reduced OCR, increased ECAR, and profile of intermediate metabolites in metabolomics. In the KO cells, the ATP synthase activity is supposed to be enhanced in mitochondria in the absence of ATPIF1, which might increase ATP hydrolysis in the energy deficient conditions. However, those possibilities were
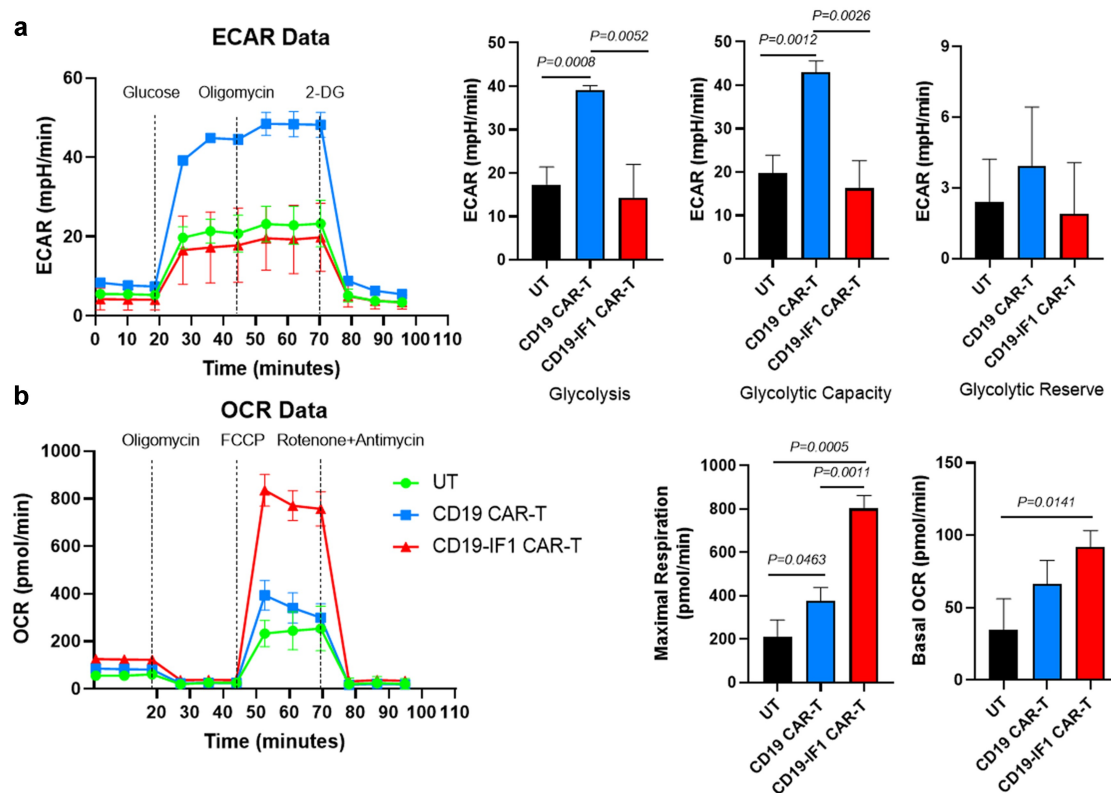
Figure 7. ATPIF1 overexpression in CAR-T cells reprogrammed metabolism for a fall in glycolysis and rise in OXPHOS. (a) Extracellular acidification rate (ECAR) in the cells of UT, CD19 CAR-T and CD19-IF1 CAR-T. The glycolysis, glycolytic capacity and glycolytic reserve were calculated in the cells at the basal or activated states. (b) Oxygen consumption rates (OCR) in the resting cells of UT, CD19 CAR-T and CD19-IF1 CAR-T. Spare Respiratory Capacity (SRC) of the cells in resting or activated states were calculated and plotted.

disproved by our data as mitochondrial function was reduced by ATPIF1 inactivation. The mechanism underlying the KO phenotype is related a change in mitochondrial structure and mass. ATPIF1 is important in the maintenance of mitochondrial biogenesis and crista density,[20,26] and ATPIF1 gene knockdown was reported to decrease the mitochondrial crista.[33] Our data suggest that mitochondrial mass was decreased in the KO cells. The enhanced glycolysis is likely a consequence of mitochondrial deficiency in KO T cells. The OXPHOS deficiency is a driving force for the induction of glycolysis.[34]

Glycolysis is required for T cell proliferation and production of cytokines including IFN-γ.[35] According to this principle, KO T cells should have an enhanced function in the presence of more glycolysis. However, the RNA-seq, scRNA-seq, and flow cytometry data consistently support that the T cell activities were decreased in the KO mice. The potential mechanism is that the mitochondrial deficiency from ATPIF1 inactivation made the T cells unable to function well in the tumor microenvironment. In the cell culture medium with sufficient glucose, the KO cells had a higher level of ATP from enhanced glycolysis. This result may not apply to the tumor-infiltrating T cells for limited glucose supply in the solid tumor, which suggests that T cells of KO mice might have a low level of ATP in the solid tumor. The mitochondrial deficiency reduces cell ability to use other energy substrates (such as fatty acids and amino acids) except glucose in the production of ATP.[36,37] This possibility may be responsible for the elevated exhaustion,

reduced proliferation, and down-regulated IFN-γ production in the KO T cells, which were found in the KO mice.

Energy metabolism could significantly impact the differentiation and maintenance of T cell subsets.[38,39] Elevated glycolysis could impair the antitumor activity by driving the CD8+ T cells toward a terminally differentiated state, while inhibition of glycolysis preserves the formation of long-lived memory CD8+ T cells.[40,41] Therefore, the decreased percentage of T_{CM} in the KO mice might be a result of the elevated glycolysis. OXPHOS is essential for the maintenance of CD8+ T memory cells, and the decreased OXPHOS may explain the exhaustion of CD8+ T cells in the KO mice.

The immune phenotype was supported by the ATPIF1 overexpression study. CAR-T cells were used in the investigation of ATPIF1 overexpression, which was conducted in anti-CD19 CAR-T cells. Proliferation and antitumor efficacy of the CAR-T cells were not influenced by the overexpression *in vitro*. However, IFN-γ expression was enhanced together with granzyme-B expression by the overexpression. A recent study reports that IL-2 is a factor for induction of T cell exhaustion.[42] IL-2 expression was decreased by the overexpression, which may count for the reduced exhaustion in the overexpression cells. The expression patterns of exhaustion markers (PD-1, LAG-3, and TIM-3) were different between CD4+ and CD8+ T cells with a reduction in CD4+ cells and an increase in CD8+ cells. Interestingly, the percentage of CD4+ and CD8+ CAR-T in total cells were changed by the overexpression, which is likely a result of alterations in cell
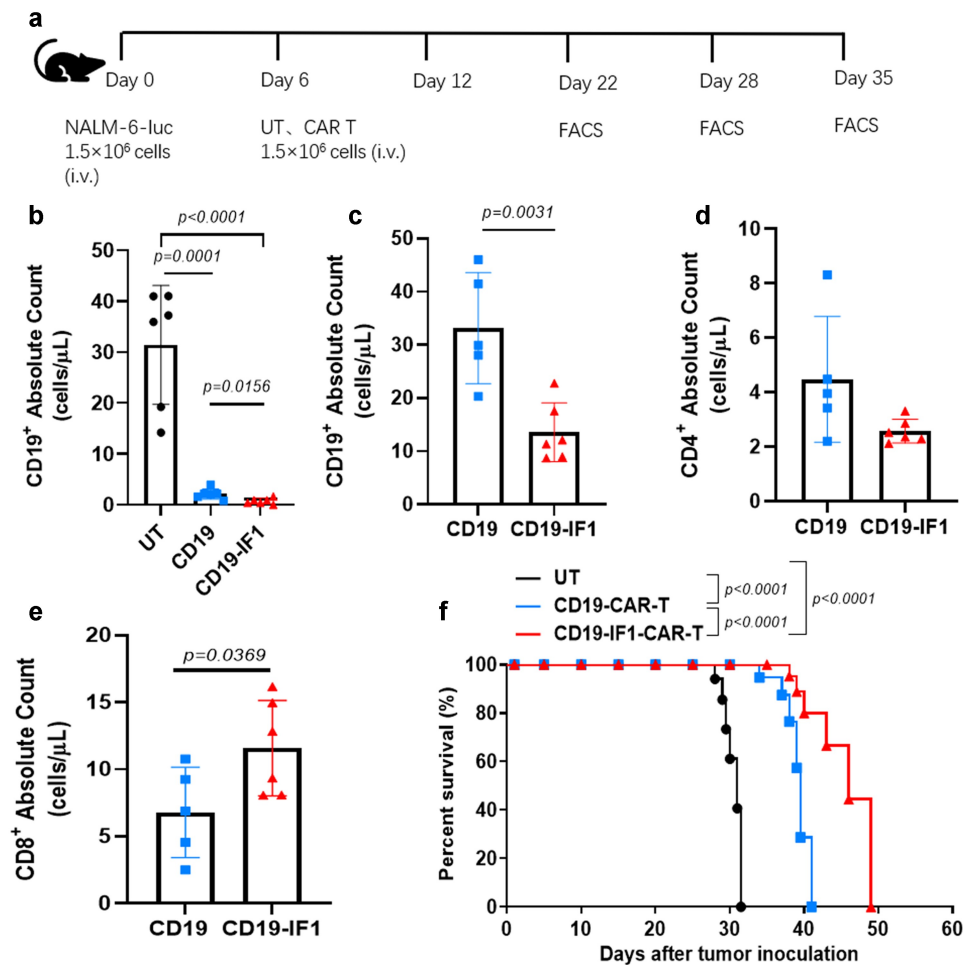
Figure 8. ATPIF1 overexpression CAR-T cells increased survival of tumor-bearing NCG mice. (a) Schedule of in vivo animal experiment. (b) Absolute count of leukemia cells (CD19$^+$ NALM-6 cells) in mice at the day 22 after tumor implantation. (c) Absolute count of CD19$^+$ NALM-6 cells in mice at the day 28 after implantation. (d) and (e), the absolute count of CD4$^+$ and CD8$^+$ T cells in mouse PBMC at the day 35 after implantation. (f) the survival curve of mice in the three group as indicated (n = 6).

proliferation and subset differentiation in response to the tumor cells. Moreover, the T_{CM} and T_{SCM} were all increased by the ATPIF1 overexpression, which is able to increase the mitochondrial crista density[33] and therefore increase the mitochondrial OXPHOS. These effects provide a mechanism for the increased T_{CM} and T_{SCM} in the overexpression cells. It is reported that mitochondrial function promotes proliferation of the two subsets.[43] The subsets of T_{CM} and T_{SCM} have superior persistence in antitumor efficacy over the subsets of T_{EM} and T_{EFF}.[44] The increased percentage of T_{CM} and T_{SCM} provides a mechanism for the superior antitumor immunity of the overexpression cells against the CD19$^+$ B leukemia.

In summary, the current study reveals a novel activity of ATPIF1 in T cells for metabolic reprogramming and functional modulation. The inactivation of ATPIF1 impaired the tumor immunity in the KO mice obseerved for a faster tumor growth, which occured by decreasing the CD8$^+$ T cell activities in several aspects including proliferation, exhaustion, cytokine production, and subset composition. The functional changes were associated with decreased OXPHOS in metabolic reprogramming of T cells. The subsets of effector and memory CD8$^+$ T cells displayed a rise in exhaustion in the tumor microenvironment in the immune

deficiency. In contrast, ATPIF1 overexpression enhanced the T cell-mediated tumor immunity and extended the life span of tumor-bearing mice. These data suggest that ATPIF1 protein is required for the maintenance of CD8$^+$ cell activities in the physiological conditions. ATPIF1 represents a potential molecular target in the induction of CD8$^+$ T cell activities in the cancer immunotherapy. The ATPIF1 effects may not be restricted to CD8$^+$ T cells, and the alterations in other immune cells (such as CD4 T cells, macrophages, and dendritic cells) may contribute to the tumor immune phenotype of KO mice.

Acknowledgments

Disclosure statement

Author contributions

Funding

References

1. Patsoukis N, Bardhan K, Chatterjee P, Sari D, Liu B, Bell LN, Karoly ED, Freeman GJ, Petkova V, Seth P, et al. PD-1 alters T-cell metabolic reprogramming by inhibiting glycolysis and promoting lipolysis and fatty acid oxidation. Nat Commun. 2015;6(1):6692. doi:10.1038/ncomms7692.

2. Kishton RJ, Sukumar M, Restifo NP. Metabolic regulation of T cell longevity and function in tumor immunotherapy. Cell Metab. 2017;26(1):94–109. doi:10.1016/j.cmet.2017.06.016.

3. Chang CH, Qiu J, O'Sullivan D, Buck MD, Noguchi T, Curtis JD, Chen Q, Gindin M, Gubin MM, van der Windt GJ, et al. Metabolic competition in the tumor microenvironment is a driver of cancer progression. Cell. 2015;162(6):1229–1241. doi:10.1016/j.cell.2015.08.016.

4. Chang CH, Pearce EL. Emerging concepts of T cell metabolism as a target of immunotherapy. Nat Immunol. 2016;17(4):364–368. doi:10.1038/ni.3415.

5. Li X, Wenes M, Romero P, Huang SC, Fendt SM, Ho PC. Navigating metabolic pathways to enhance antitumour immunity and immunotherapy. Nat Rev Clin Oncol. 2019;16(7):425–441. doi:10.1038/s41571-019-0203-7.

6. Yerinde C, Siegmund B, Glauben R, Weidinger C. Metabolic control of epigenetics and its role in CD8+ T cells differentiation and function. Front Immunol. 2019;10:2718. doi:10.3389/fimmu.2019.02718.

7. Franco F, Jaccard A, Romero P, Yu YR, Ho PC. Metabolic and epigenetic regulation of T-cell exhaustion. Nat Metab. 2020;2(10):1001–1012. doi:10.1038/s42255-020-00280-9.

8. Leone RD, Powell JD. Metabolism of immune cells in cancer. Nat Rev Cancer. 2020;20(9):516–531. doi:10.1038/s41568-020-0273-y.

9. García-Aguilar A, Cuezva JM. A review of the inhibition of the mitochondrial ATP synthase by IF1 in vivo: reprogramming energy metabolism and inducing mitohormesis. Front Physiol. 2018;9:1322. doi:10.3389/fphys.2018.01322.

10. Goldberg J, Currais A, Prior M, Fischer W, Chiruta C, Ratliff E, Daugherty D, Dargusch R, Finley K, Esparza-Molto PB, et al. The mitochondrial ATP synthase is a shared drug target for aging and dementia. Aging Cell. 2018;17(2):e12715. doi:10.1111/acel.12715.

11. Gu J, Zhang L, Zong S, Guo R, Liu T, Yi J, Wang P, Zhuo W, Yang M. Cryo-EM structure of the mammalian ATP synthase tetramer bound with inhibitory protein IF1. Science. 2019;364(6445):1068–1075. doi:10.1126/science.aaw4852.

12. Wang K, Chen H, Zhou Z, Zhang H, Zhou H, Min W. ATPIF1 maintains normal mitochondrial structure which is impaired by CCM3 deficiency in endothelial cells. Cell Biosci. 2021;11(1):11. doi:10.1186/s13578-020-00514-z.

13. Nakamura J, Fujikawa M, Yoshida M. IF1, a natural inhibitor of mitochondrial ATP synthase, is not essential for the normal growth and breeding of mice. Biosci Rep. 2013;33(5):e00067. doi:10.1042/BSR20130078.

14. Wang Y, Zhang J, Cao X, Guan Y, Shen S, Zhong G, Xiong X, Xu Y, Zhang X, Wang H, et al. Mitochondrial protein IF1 is a potential regulator of glucagon-like peptide (GLP-1) secretion function of the mouse intestine. Acta Pharm Sin B. 2021;11(6):1568–1577. doi:10.1016/j.apsb.2021.02.002.

15. Zhong G, Zhang J, Guo Y, Wang Y, Wu M, Ren J, Li Y, Zhang X, Zhou B, Zhao W, et al. IF1 inactivation attenuates experimental colitis through downregulation of neutrophil infiltration in colon mucosa. Int Immunopharmacol. 2021;99:107980. doi:10.1016/j.intimp.2021.107980.

16. Formentini L, Pereira MP, Sanchez-Cenizo L, Santacatterina F, Lucas JJ, Navarro C, Martinez-Serrano A, Cuezva JM. In vivo inhibition of the mitochondrial H+-ATP synthase in neurons promotes metabolic preconditioning. EMBO J. 2014;33(7):762–778. doi:10.1002/embj.201386392.

17. Shah DI, Takahashi-Makise N, Cooney JD, Li L, Schultz IJ, Pierce EL, Narla A, Seguin A, Hattangadi SM, Medlock AE, et al. Mitochondrial Atpif1 regulates haem synthesis in developing erythroblasts. Nature. 2012;491(7425):608–612. doi:10.1038/nature11536.

18. Formentini L, Santacatterina F, Nunez de Arenas C, Stamatakis K, Lopez-Martinez D, Logan A, Fresno M, Smits R, Murphy MP, Cuezva JM. Mitochondrial ROS production protects the intestine from inflammation through functional M2 macrophage polarization. Cell Rep. 2017;19(6):1202–1213. doi:10.1016/j.celrep.2017.04.036.

19. Santacatterina F, Sanchez-Cenizo L, Formentini L, Mobasher MA, Casas E, Rueda CB, Martinez-Reyes I, Nunez de Arenas C, Garcia-Bermudez J, Zapata JM, et al. Down-regulation of oxidative phosphorylation in the liver by expression of the ATPase inhibitory factor 1 induces a tumor-promoter metabolic state. Oncotarget. 2016;7(1):490–508. doi:10.18632/oncotarget.6357.

20. Faccenda D, Nakamura J, Gorini G, Dhoot GK, Piacentini M, Yoshida M, Campanella M. Control of mitochondrial remodeling by the ATPase inhibitory factor 1 unveils a pro-survival relay via OPA1. Cell Rep. 2017;18(8):1869–1883. doi:10.1016/j.celrep.2017.01.070.

21. Zhang Q, He Y, Luo N, Patel SJ, Han Y, Gao R, Modak M, Carotta S, Haslinger C, Kind D, et al. Landscape and dynamics of single immune cells in hepatocellular carcinoma. Cell. 2019;179(4):829–845 e820. doi:10.1016/j.cell.2019.10.003.

22. Zheng C, Zheng L, Yoo JK, Guo H, Zhang Y, Guo X, Kang B, Hu R, Huang JY, Zhang Q, et al. Landscape of infiltrating T cells in liver cancer revealed by single-cell sequencing. Cell. 2017;169(7):1342–1356 e1316. doi:10.1016/j.cell.2017.05.035.

23. Ren J, Yan D, Wang Y, Zhang J, Li M, Xiong W, Jing X, Li P, Zhao W, Xiong X, et al. Inhibitor of differentiation-2 protein ameliorates DSS-induced ulcerative colitis by inhibiting NF-κB activation in neutrophils. Front Immunol. 2021;12:760999. doi:10.3389/fimmu.2021.760999.

24. Cao X, Zhang X, Ye J. Regulation of mitochondrial ATP synthase inhibitor 1 in cellular energy metabolism. Chin J Cell Biol. 2020;42:682–690. in Chinese.

25. Sivandzade F, Bhalerao A, Cucullo L. Analysis of the mitochondrial membrane potential using the cationic JC-1 dye as a sensitive fluorescent probe. Bio Protoc. 2019;9(1):e3128. doi:10.21769/BioProtoc.3128.

26. Weissert V, Rieger B, Morris S, Arroum T, Psathaki OE, Zobel T, Perkins G, Busch KB. Inhibition of the mitochondrial ATPase function by IF1 changes the spatiotemporal organization of ATP synthase. Biochim Biophys Acta Bioenerg. 2021;1862(1):148322. doi:10.1016/j.bbabio.2020.148322.

27. van der Windt GJW, Everts B, Chang CH, Curtis J, Freitas T, Amiel E, Pearce E, Pearce E. Mitochondrial respiratory capacity is a critical regulator of CD8+ T cell memory development. Immunity. 2012;36(1):68–78. doi:10.1016/j.immuni.2011.12.007.

28. Corrado M, Pearce EL. Targeting memory T cell metabolism to improve immunity. J Clin Invest. 2022;132(1):e148546. doi:10.1172/JCI148546.

29. Azizi E, Carr AJ, Plitas G, Cornish AE, Konopacki C, Prabhakaran S, Nainys J, Wu K, Kiseliovas V, Setty M, et al. Single-cell map of diverse immune phenotypes in the breast tumor

microenvironment. Cell. 2018;174(5):1293–1308 e1236. doi:10.1016/j.cell.2018.05.060.

30. June CH, Sadelain M. Chimeric antigen receptor therapy. N Engl J Med. 2018;379(1):64–73. doi:10.1056/NEJMra1706169.

31. Cannarile MA, Lind NA, Rivera R, Sheridan AD, Camfield KA, Wu BB, Cheung KP, Ding Z, Goldrath AW. Transcriptional regulator Id2 mediates CD8+ T cell immunity. Nat Immunol. 2006;7 (12):1317–1325. doi:10.1038/ni1403.

32. Masson F, Minnich M, Olshansky M, Bilic I, Mount AM, Kallies A, Speed TP, Busslinger M, Nutt SL, Belz GT, et al. Id2-mediated inhibition of E2A represses memory CD8 + T cell differentiation. J Immunol. 2013;190(9):4585–4594. doi:10.4049/jimmunol.1300099.

33. Capanella M, Casswell E, Chong S, Farah Z, Wieckowski MR, Abramov AY, Tinker A, Duchen MR. Regulation of mitochondrial structure and function by the F1Fo-ATPase inhibitor protein, IF1. Cell Metab. 2008;8(1):13–25. doi:10.1016/j.cmet.2008.06.001.

34. Liu S, Liu S, He B, Li L, Li L, Wang J, Cai T, Chen S, Jiang H. OXPHOS deficiency activates global adaptation pathways to maintain mitochondrial membrane potential. EMBO Rep. 2021;22(4): e51606. doi:10.15252/embr.202051606.

35. Chang CH, Curtis JD, Maggi LBsJr., Faubert B, Villarino AV, O'Sullivan D, Huang SC, van der Windt GJ, Blagih J, Qiu J, et al. Posttranscriptional control of T cell effector function by aerobic glycolysis. Cell. 2013;153(6):1239–1251. doi:10.1016/j.cell.2013.05.016.

36. Burgin HJ, McKenzie M. Understanding the role of OXPHOS dysfunction in the pathogenesis of ECHS1 deficiency. FEBS Lett. 2020;594(4):590–610. doi:10.1002/1873-3468.13735.

37. Peng M, Huang Y, Zhang L, Zhao X, Hou Y. Targeting mitochondrial oxidative phosphorylation eradicates acute myeloid leukemic stem cells. Front Oncol. 2022;12:899502. doi:10.3389/fonc.2022.899502.

38. Almeida L, Lochner M, Berod L, Sparwasser T. Metabolic pathways in T cell activation and lineage differentiation. Semin Immunol. 2016;28(5):514–524. doi:10.1016/j.smim.2016.10.009.

39. Ranger Rivera GO, Knochelmann HM, Dwyer CJ, Smith AS, Wyatt MM, Rivera-Reyes AM, Thaxton JE, Paulos CM. Fundamentals of T cell metabolism and strategies to enhance cancer immunotherapy. Front Immunol. 2021;12:645242. doi:10.3389/fimmu.2021.645242.

40. Sukumar M, Liu J, Ji Y, Subramanian M, Crompton JG, Yu Z, Roychoudhuri R, Palmer DC, Muranski P, Karoly ED, et al. Inhibiting glycolytic metabolism enhances CD8+ T cell memory and antitumor function. J Clin Invest. 2013;123(10):4479–4488. doi:10.1172/JCI69589.

41. Tabilas C, Wang J, Liu X, Locasale JW, Smith NL, Rudd BD. Cutting edge: elevated glycolytic metabolism limits the formation of memory CD8 + T cells in early life. J Immunol. 2019;203 (10):2571–2576. doi:10.4049/jimmunol.1900426.

42. Liu Y, Zhou L, Wang J, Wang J, Zhou Y, Zhang T, Fang Y, Deng J, Gao Y, Liang X, et al. IL-2 regulates tumor-reactive CD8 + T cell exhaustion by activating the aryl hydrocarbon receptor. Nat Immunol. 2021;22(3):358–369. doi:10.1038/s41590-020-00850-9.

43. Kawalekar OU, O'Connor RS, Fraietta JA, Guo L, McGettigan SE, Posey AD, Patel PR, Guedan S, Scholler J, Keith B, et al. Distinct signaling of coreceptors regulates specific metabolism pathways and impacts memory development in CAR T cells. Immunity. 2016;44(2):380–390. doi:10.1016/j.immuni.2016.01.021.

44. Liu Q, Sun Z, Chen L. Memory T cells: strategies for optimizing tumor immunotherapy. Protein Cell. 2020;11(8):549–564. doi:10.1007/s13238-020-00707-9.